1.5 and 2.3 μm Diode Laser Arrays for Optical Pumping

[a*]A.Gourevitch, [a]G.Belenky, [a]L. Shterengas, [a]D. Donetsky, [b]D. Westerfeld,
[b†]B. Laikhtman, [c]R. U. Martinelli, [c]G. Kim
[a]State University of New York at Stony Brook, Stony Brook, NY 11794-2350 USA;
[b]Power Photonic, Stony Brook, NY 11794-3717 USA;
[c]Sarnoff Corporation, 201 Washington Rd., Princeton, NJ 08543 USA

ABSTRACT

High wall-plug efficiency and a wide range of available wavelengths make laser diode arrays preferable for many high-power applications, including optical pumping of solid state lasers. Recently, we designed and fabricated InGaAsP/InP arrays operating at 1.5-μm and In(Al)GaAsSb/GaSb arrays operating at 2.3-μm. We have demonstrated a high continuous-wave (CW) output power of 25 W from a one dimensional laser array and a quasi-CW (q-CW) output power of 110 W from a two dimensional laser array both operating near 1.5-μm. We have obtained a CW output power of 10 W from the 2.3-μm laser array.

The 1.5-μm arrays are suitable for resonant pumping of erbium doped solid-state lasers, which require high power optical sources emitting in the narrow erbium absorption bands. Long current-injection pulses produce a considerable temperature increase within the diode laser structure which induces a red-shift of the output wavelength. This thermal drift of the laser array emission spectrum can lead to misalignment with the erbium absorption bands, which decreases pumping efficiency. We have developed an experimental technique to measure the time dependence of the laser emission spectrum during a single current pulse. From the red-shift of the laser emission, we determine the temperature of the laser active region as a function of time.

The spacing between the individual laser emitters has an effect on the array heating. In steady state operation, this spacing is a contributing factor in the non-uniformity of the thermal field within the bar, and thus to the overall thermal resistance of the laser bar. Under pulse operation, the transient heating process can be divided into three time periods; each with its own heat transport condition. It was shown that in the initial period of time the heat propagates within the laser bar structure and the laser bar design (fill factor) strongly affects the active region temperature rise. In the later periods the temperature kinetics is insensitive to the fill factor. This analysis has been verified in experimental studies using the 1.5-μm laser arrays.

1. INTRODUCTION

We have recently developed high power mid-IR laser arrays suitable for optical pumping of solid state and semiconductor lasers. Lasers emitting at 1.5-μm have applications in the resonant pumping of erbium doped solid state lasers [1-4] and lasers operating at 2.3-μm have potential for the optical pumping of type II semiconductor lasers [5]. We are reporting a high continuous-wave (CW) output power of 10 W from a one-dimensional (1-D) laser array operating at 2.3-μm and 110 W quasi-CW (5 ms pulse duration, 20 Hz pulse repetition frequency) output power from two-dimensional (2-D) laser array operating at 1.5-μm.

One of the key problems of high-power array design is managing the large heat dissipation in the relatively small array volume. High active region temperatures limit the laser array performance by decreasing output power, reducing the device lifetime and diminishing the overall pumping efficiency. The overheating of laser arrays can be significantly reduced by optimizing the laser heterostructure design, improving the heat sinking, and refining the laser bar design. One aspect of the laser bar design optimization is the optimization of the laser bar fill factor (FF), which is defined as the ratio

* *gourevitch@ece.sunysb.edu*

† Permanent address: Racah Institute of Physics, Hebrew University, Jerusalem, 91904, Israel.

Lidar Remote Sensing for Environmental Monitoring VI, edited by Upendra N. Singh,
Proc. of SPIE Vol. 5887 (SPIE, Bellingham, WA, 2005) · 0277-786X/05/$15 · doi: 10.1117/12.620001

of pumped bar area to total bar area. In this work we have focused our study on the influence of the fill factor on the overheating of laser arrays in steady state and pulsed operation.

Increased active region temperature enhances carrier escape through thermionic emission and increases the rate of non-radiative recombination processes [6]. This causes an efficiency reduction and threshold current increase, resulting in an output power decrease with temperature. In recent years, several groups have reported on optimization of laser array designs to maximize the output power in different operating regimes [7-9]. It was shown that arrays with high emitter density (large fill factor) are preferred for short-pulse high peak power operation [10-11], while arrays with low emitter density (small fill factor) are favorable for long-pulse, high average power operation [12].

Another important issue for laser array performance is the device reliability. Numerous aging tests have shown that the degradation mechanisms are enhanced at high operational temperatures, and the device lifetime decreases exponentially with active region temperature [13]. Recently, we developed an analytical model to find the optimal laser bar design, which provides the minimal active region temperature rise at a given steady state output power. It was shown that the optimal fill factor design depends on the operational regime and that high output power operation favors high fill factors. [14]

The optical pumping of solid state lasers requires high power sources that can reliably provide a large fraction of their output energy into the crystal absorption bands. This requirement is especially challenging for resonant pumping of erbium doped solid state lasers in the narrow absorption bands near 1.5-μm. The erbium fluorescence lifetime of about 5-10 ms favors relatively long pump pulses [15-16]. The millisecond-long current-injection pulses produce a considerable temperature increase within the diode laser structure that induces a red-shift of the output wavelength. The thermal drift of the laser array emission spectra can lead to a misalignment with the narrow erbium absorption bands and a decrease of the pumping efficiency.

In this work we report on the performance and thermal behavior of laser bars mounted in bar-in-groove heat spreaders. In section II, the design and performance of laser arrays operating at 1.5-μm and 2.3-μm are discussed. The thermal analysis of high-power laser arrays in steady-state and pulse operation is presented in Sections III and IV.

2. DESIGN AND PERFORMACE OF *1.5-μm* AND 2.3-*μm* LASER ARRAYS

The design of both lasers has been optimized for high-power operation using broadened-waveguide layers sandwiched between highly doped cladding layers. The broadened waveguide approach reduces the optical loss and threshold current, while the high doped cladding layers decreases the excess voltage drop across the laser heterostructure.

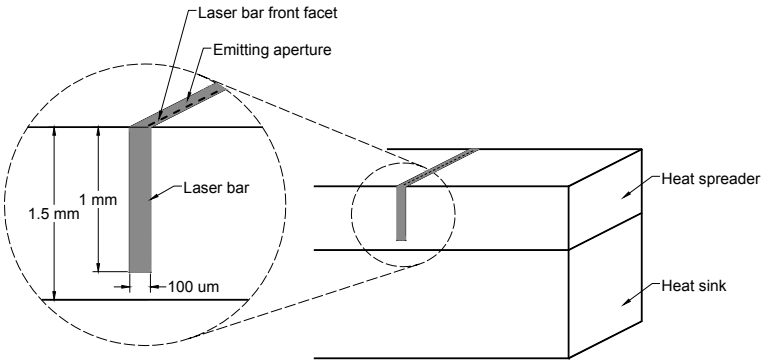

Figure 1: Schematic diagram of a laser diode array assembly showing a laser bar mounted in a grooved heat spreader.

The InP and GaSb-based laser bars were mounted in the same type of heat sink assembly as in Figure 1. One dimensional (one bar) and two dimensional (several bars) arrays were fabricated by mounting the bars in metallized grooves in 1.5 mm thick BeO heat spreader blocks which were bonded on water-cooled micro channel heat sinks. We used 1-cm-long laser bars containing equally spaced 100-μm-wide emitters with different center-to-center distances, yielding different fill factors. The laser cavities were 1 mm long to fit the standard heat sink. The front and back facets were anti-reflection and high-reflection coated. The BeO heat spreader is much thicker that the laser bars, whose

thickness is around 100 μm. The heat flux propagation is mostly determined by the relatively thick heat spreader, and is similar regardless of the laser bar materials. For this reason, we studied the thermal properties of InP-based 1.5-μm laser bars; the results can be applied to any other laser bars simply by considering the appropriate laser bar power dissipation.

2.1 Laser Arrays Operating at 1.5-μm

The InGaAsP/InP heterostructures emitting at 1.5-μm were grown by metalloorganic chemical vapor deposition. The laser heterostructure consists of a two-index-step, 710-nm-thick waveguide incorporated between n and p clad layers, each 1.5 μm thick. The n-cladding was doped with Se to the concentration of $5x10^{17}$ cm^{-3} and the p-cladding was Zn doped to an average concentration of $7.5x10^{17}$ cm^{-3}. The active region contains three 6-nm-thick InGaAsP QWs with 1% compressive strain separated by 16-nm-thick InGaAsP barriers. The total thickness of the laser bar structure including the substrate was ~140 μm. All layers except the quantum wells were grown lattice matched to the InP substrate. Details of the laser heterostructure were reported elsewhere [17-18].

Figure 2a shows the current dependencies of the CW and q-CW (5 ms pulse duration, 20 Hz pulse repetition frequency) output power and the wall-plug efficiency for a 1-D diode array with 20 % FF at a coolant temperature of 16 °C. The output power was recorded using a 50-mm-diameter thermopile detector. The slope efficiency of 0.5 W/A remained constant in q-CW mode up to the measured output power of 27 W. Optical output power rollover in CW mode was observed when the drive current exceeded 40 A. The maximum wall-plug efficiency was 37 % at 40 A, and was better than 34 % up to the maximum applied drive current of 60 A. The inset shows the integrated emission spectrum of the array measured at an 18-°C coolant temperature. The full-width at half-maximum of the emission spectrum was about 8 nm. The 2-D array was fabricated by mounting 4 bars with 20 % FFs with a bar-to-bar pitch of 3.2 mm. The 4 bars were electrically connected in series. An output power of 110 W was achieved at 60 A drive current in 5 ms, 20 Hz q-CW mode, Figure 2b. The inset shows the integrated emission spectrum of a 2-D array. The full-width at half-maximum of the emission spectra was about 10 nm.

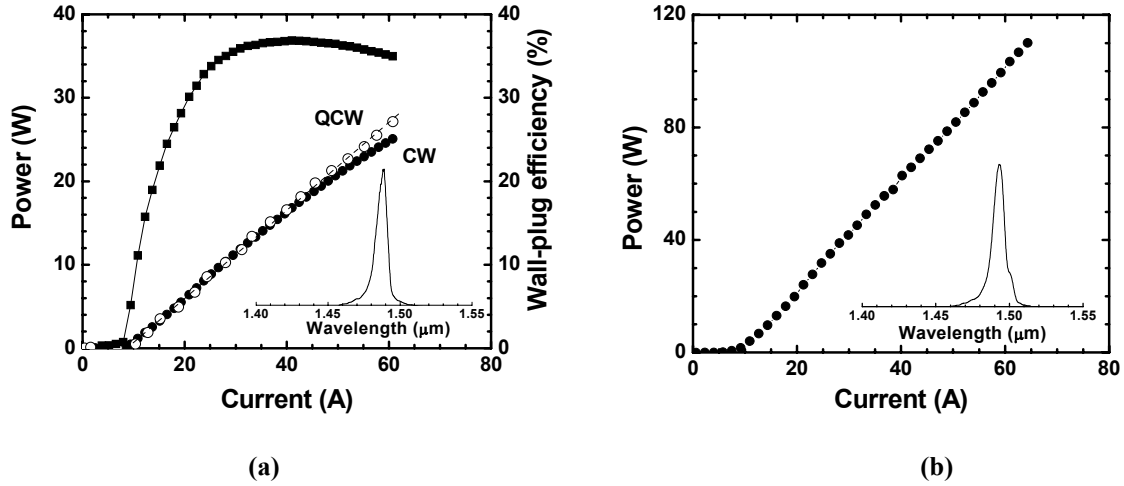

Figure 2: (a) Output power (circles) and wall-plug efficiency (squares) of a 1.5-μm 1-D array operated in q-CW (open symbols) and CW (closed symbols) modes at a coolant temperature of 16 °C. Inset demonstrates integrated emission spectrum of the array measured at 40 A and 18 °C. (b) Output power of a 2-D array operated in the q-CW mode at 18 °C. Inset demonstrates integrated emission spectrum of a 2-D array recorded at 40 A and 18 °C.

2.2 Laser Array Operating at 2.3-μm

The 2.3-μm laser heterostructure was grown by solid-source molecular-beam epitaxy on n-GaSb substrates. An ~800-nm-thick $Al_{0.25}Ga_{0.75}As_{0.02}Sb_{0.98}$ broadened-waveguide layer with two InGaAsSb quantum wells (QWs) was sandwiched between 2-μm-thick $Al_{0.9}Ga_{0.1}As_{0.07}Sb_{0.93}$ n and p cladding layers. The n-cladding layer was Te-doped to 3 x 10^{17} cm^{-3}, and the p-cladding layer was Be-doped to 1 x 10^{18} cm^{-3} over the first 0.2 μm and to 5 x 10^{18} cm^{-3} over the remaining 1.8 μm. The details of the laser heterostructure design can be found elsewhere [5].

The maximum CW power of 10 W was obtained from a 1D array with a 20 % fill factor at 70 A and 18 °C, as shown in Figure 3. The CW output power increased sublinearly at drive currents beyond about 40 A. The spectrum was centered near 2.36 μm with a FWHM of about 20 nm at 30 A CW and 18-°C coolant temperature, as shown in the inset.

In the q-CW mode (30 μs, 300 Hz) the array output was 18.5 W peak power at a current of 100 A at 18-°C coolant temperature. In the short-pulse, low-duty-cycle mode (200 ns, 750 Hz), the output power of 20 W was obtained at room temperature.

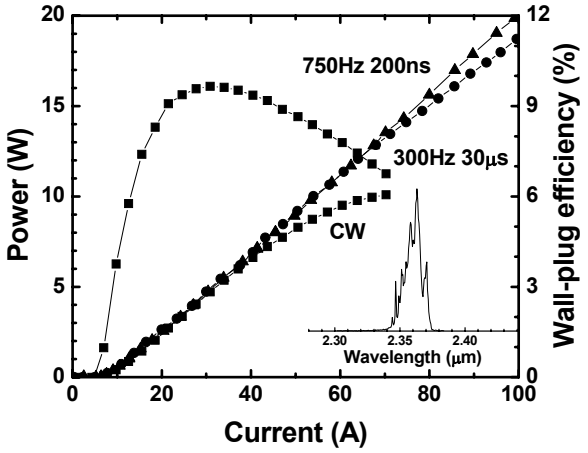

Figure 3: Current characteristics of output-power and wall-plug efficiency of 2.3-μm laser linear array. The light–current characteristics in CW and q-CW were measured at 18-°C coolant temperature and at room temperature (uncooled) in short pulse operation. The inset shows the laser array emission spectrum measured at 30-A drive current and 18-°C coolant temperature in CW operation.

3. Steady-State Thermal Analysis of High Power Laser Arrays

While more efficient than almost any other optical source, the limited wall-plug efficiency of high power laser arrays leads to a considerable amount of heat generated under high power steady state operation. To reduce array overheating, the common approach is to increase the area through which the heat is dissipated (thermal foot print). The thermal foot print can be enlarged by extending the cavity length, or increasing the number of emitters. For the array architecture of Figure 1, a cavity length increase requires thicker heat spreader blocks. The thicker heat spreader leads to a longer heat propagation length towards the heat sink and higher thermal gradient along the cavity length. [1, 14].

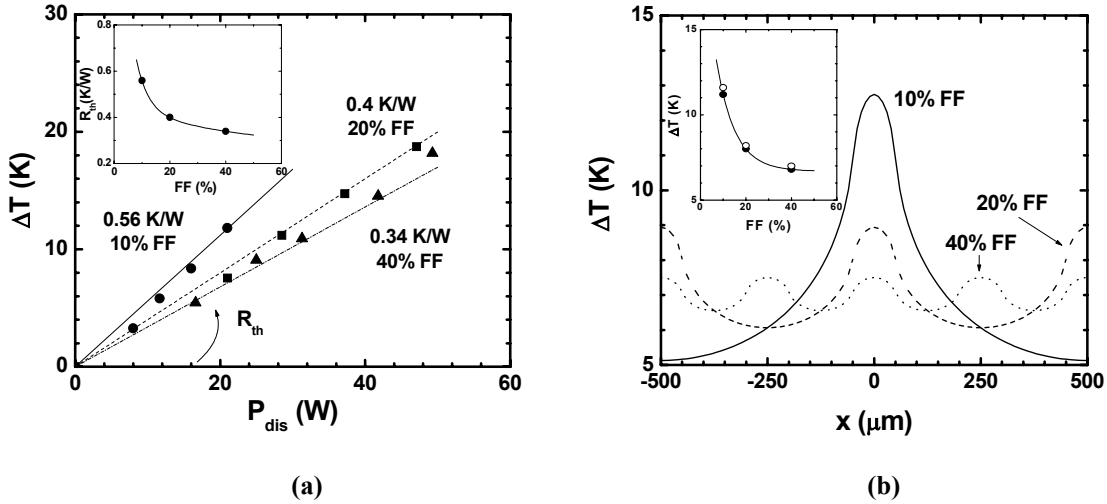

Figure 4: (a) The experimentally measured active-region temperature rise as a function of dissipated power is shown for different fill factor arrays. The inset shows the dependence of the thermal resistance on fill factor. (b) Active-region temperature distribution over 1 mm of a 1cm long laser bar with different fill factors at the total dissipated power of 20 W. The inset demonstrates the analytical (solid symbols) and experimental (open symbols) average temperature change for different FFs at given total dissipated power of 20 W.

The electrically pumped active region area of the laser bar can be efficiently increased by reducing the distance between adjacent stripes of constant width (i.e. by increasing the fill factor). However, decreasing the separation between adjacent emitters can lead to increased mutual heating. The effect of fill factor on overheating is considered in this section.

To study the influence of laser bar design on overheating we fabricated InP-based arrays with fill factors of 10, 20 and 40 % and measured the dependence of the active region temperature change on dissipated power (P_{dis}), which is defined as the difference between input electrical power and output optical power. The overheating of the laser active region was obtained by measuring the emission spectrum red-shift. As can be seen in the Figure 4a, the active-region temperature depends linearly on dissipated power with the thermal resistance as the coefficient of proportionality. The thermal resistances of 0.56, 0.4, and 0.34 K/W were experimentally determined for 10, 20 and 40 % fill factor arrays, respectively. The thermal resistance was found to be significantly decreased by increasing fill factor from 10 % to 20 % and changed much less with further fill factor increases. The inset shows this decreasing dependence of thermal resistance on fill factor, which saturates at high FF.

This dependence of the thermal resistance on the fill factor results from a nonuniform temperature distribution in the laser bar. To clarify the experimental results, we developed an analytical model based on the solution of the heat conduction equation with non-trivial boundary conditions defined by the geometry of laser array. Figure 4b shows the analytically calculated temperature distribution of a 1-mm section of a 10-mm laser bar for fill factors of 10, 20, and 40 %, at 20 W total dissipated power per bar. As the fill factor goes up the temperature goes down in the regions close to the emitters, due to decreasing the dissipated power per stripe, and goes up in the regions between emitters, due to increasing mutual heating between adjacent emitters. The temperature distribution becomes more homogenous along the bar with increasing FF, reducing the influence of fill factor on the thermal resistance. In the inset of Figure 4a we compared the analytic results for average active region temperature rise versus fill factor with the experimental results, and found good agreement.

4. Transient Thermal Analysis of High Power Laser Arrays

Previously, we considered laser array heating in steady state operation; however, some applications require pulse operation. In the following sections we analyze the thermal performance of laser arrays in pulse operation and the influence of laser bar design on array thermal kinetics.

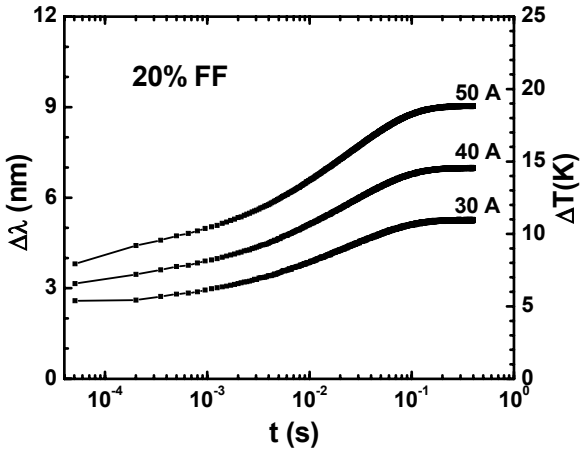

Figure 5: Time dependence of average wavelength shift (left axis) and the corresponding active region temperature change (right axis) for a laser diode array with a 20 % fill factor.

4.1 Measurements of Heating Kinetics

We developed an experimental setup for determining the temperature kinetics of laser diode arrays by measuring the temporal evolution of the laser emission spectra. The spectrum evolution was measured using a 0.5-meter grating monochromator equipped with a linear 256-pixel InGaAs photodetector. The photodetector array captured the whole laser spectrum at once without rotating the diffraction grating. Coupling of the laser emission into the monochromator

was performed using an integrating sphere. The emission spectra was recorded every 100-μs during a single current pulse. Recording all the spectra during the single current pulse eliminated errors due to pulse-to-pulse variations. For a quantitative characterization of the spectrum red-shift with heating, we computed the weighted average wavelength of each spectrum and compared the results to the weighted average wavelength of the initial spectrum [18-19].

Figure 5 shows the weighted average wavelength shift and average active region temperature change for the 20 % FF array at several different drive currents. The conversion coefficient between the wavelength shift and active region temperature was obtained by measuring the laser spectral shift under low duty cycle, short-pulse operation at a variety of heat sink temperatures. As can be seen in the Figure 5, the active region temperature increases rapidly during the initial time interval of around 100 μs. This initial temperature rise is caused by the heat accumulation in the immediate vicinity of the laser bar. Then the rate of the temperature change decreases due to transport of thermal energy throughout the entire array assembly from the laser bar structure to the microchannel cooler.

Figure 6a shows the normalized temperature change obtained by dividing the temperature change by the total bar dissipated power for arrays with different FFs. The data show that the active region temperatures (for the same dissipated power) in arrays with 10, 20 and 40 % FF are significantly different during the first few hundred microseconds. The temperature difference between the 20 % and 40 % FF arrays diminishes over time, while the 10 % FF array demonstrates higher temperatures for all times. This long-time thermal behavior correlates with the thermal resistances of the arrays determined under steady-state operation. The initial temperature rise is related with heating of laser structure and the following heating of laser array is determined by heat flux propagation through the thick heat spreader and heat sink assembly.

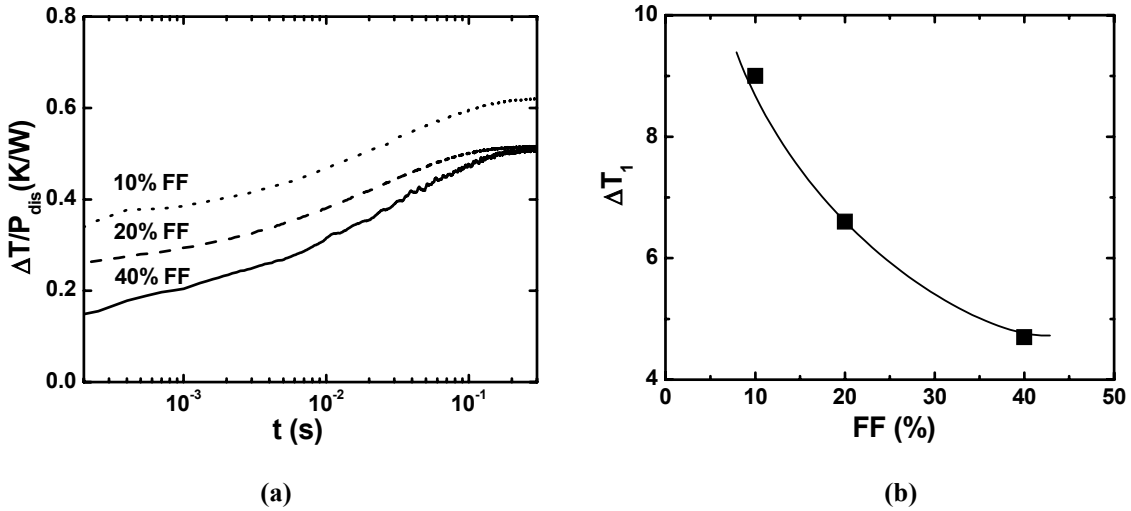

Figure 6: (a) Active region temperature rise divided by dissipated power (i.e. thermal resistance) as a function of time for different FF arrays. (b) Active-region initial temperature rise during the first 200 μs for arrays with different FFs at 25 W total dissipated power per bar.

4.2 Results and Discussion

Based on the 1.5-μm array spectral evolution measurements, three distinct periods in the transient heating process were identified. During the first period, the laser bar structure is heated and the heat fluxes from the individual stripes of the laser bar overlap to produce a nearly uniform heat flux. The second period is characterized by the propagation of the nearly uniform heat flux through the heat spreader. The heat propagation length for the second period is smaller than the heat spreader thickness. By the third period the heat flux has reached the heat sink, the entire heat spreader has been heated and the temperature distribution exponentially approaches the steady state.

To study the initial heating of laser arrays with different fill factors, the active-region temperature rise (ΔT_1) was measured for the first 200 μs. Figure 6b demonstrates the dependence of ΔT_1 on FF at 25 W total dissipated power per bar. The experimental results show that the temperature rise during the first 200 μs is highest for the array with a 10 % FF and smallest for the array with 40 % FF. In the first heating period the active-region heating is mainly determined by the power dissipation in each stripe. The dissipated power per stripe scales with the number of stripes under the condition

of constant total dissipated power in the bar. At a given dissipated power in the bar, the temperature rise decreases with fill factor. As can be seen from the Figure 6b, this decrease is not directly proportional to the number of stripes, which confirms that the lateral heat transport in the laser bar structure is responsible for the mutual heating of the adjacent emitters. This lateral heat transport leads to overlapping of heat fluxes from the active-region areas under the metal contacts in the laser bar. Since in the first period the heat fluxes from under the stripe areas have merged into a nearly uniform flux, the thermal kinetics is expected to be independent of the distance between emitters (i.e. fill factor) in the later periods.

The second period lasts until the heat flux has reached the interface between heat spreader and heat sink. To analyze the active-region temperature change during the second period, the initial temperature rise (ΔT_1) was subtracted from the measured active-region temperature. Figure 7a shows a log-log plot of the temperature change for arrays with the three different fill factors. The solid lines in Figure 7a were fit to the experimental data over the time interval from 200 μs to about 10 ms. The inset shows that the computed slopes are independent of fill factor. The slope of these fit lines is close to 0.5, indicating that the active-region temperature change increases as the square root of time.

In the third period, the active-region temperature change approaches the steady-state value (ΔT_0) with a characteristic time constant τ_c and is characterized by long-time asymptotic kinetics given by

$$(\Delta T_0 - \Delta T(t))/\Delta T_0 \sim \exp(-t/\tau_c). \quad (1)$$

In Figure 7b the normalized difference between the observed active region temperature change and the experimentally determined steady-state temperature rise (ΔT_0) is plotted in a semi-logarithmic scale for all three arrays. Figure 7b shows that for long times, t > 20 ms, the data are well approximated by the exponential time dependence given in equation 1. The slopes of the solid lines in the figure were fit to the data to calculate the time constant (τ_c), which is shown in the inset as a function of FF. The time constant is independent of fill factor, and the long-time heating kinetics of all of these arrays can be characterized with the same τ_c of about 60 ms.

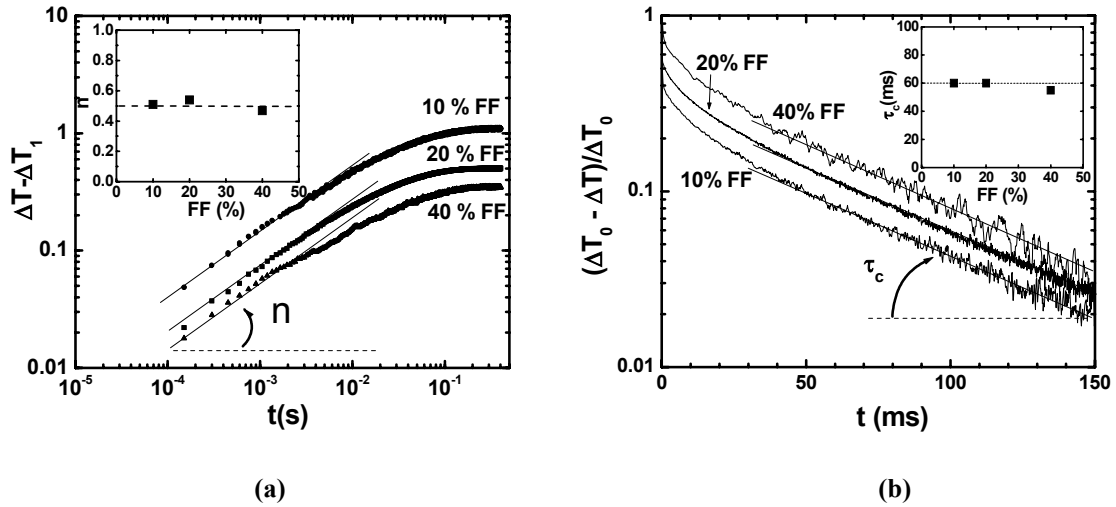

Figure 7: (a) The temperature changes are plotted on double-log axes for the three fill factors. The solid lines were fit to the experimental data over the time interval of 200 μs to 10 ms. The computed slopes are shown in the inset as a function of fill factor. (b) Normalized deviation from steady state temperature versus time is plotted for the arrays. The slopes of the solid lines are used to calculate τ_c, which is shown in the inset.

5. CONCLUSIONS

In conclusion, we report the development of high power InP-based diode arrays operating near 1.5-μm. A 25-W CW output power was obtained from a 1D array at 16 °C and 110-W q-CW power was obtained from a 2-D array at 18 °C. The maximum wall-plug efficiency of 37 % was obtained at 40 A drive current. We designed and fabricated 2.3-μm 1-D GaSb-based arrays. At 18 ºC, the laser array provides output power of 10 W in CW and 18.5 W in q-CW operations.

We studied the thermal behavior of laser arrays with different laser bar designs in steady-state and pulse operation. It was shown that in steady-state operation the thermal resistance decreases with fill factor; however, this dependency saturates at high FFs. We developed an analytical model of the temperature distribution in the laser bar active region and showed that the dependence of the thermal resistance on bar design results from the non-uniform temperature distribution. The temperature distribution becomes more homogeneous with decreasing distance between adjacent stripes due to mutual heating of adjacent lasers.

In pulse operation three distinctive periods in the transient heating process were clearly identified – an initial temperature rise, a square-root-of-time dependence of the active-region temperature increase, and an exponential approach of the active region temperature to its steady-state value. We demonstrated that in the initial period of time the heat propagates within the laser bar structure and the laser bar design (fill factor) strongly affects the active-region temperature rise. In the later periods, the temperature kinetics is insensitive to the fill factor.

ACKNOWLEDGEMENT

This material is based upon work supported by the United States Air Force under contract Nos. FA9550-04-C-0021 and FA9550-05-C-0043.

REFERENCES

1. A. Gourevitch, G. Belenky, D. Donetsky, B. Laikhtman, D. Westerfeld, C.W. Trussell, H. An, Z. Shellenbarger, R. Martinelli, *Appl. Phys. Lett*., **83**, 617 (2003)
2. P. Crump, T. Crum, M. DeVito, J. Farmer, M. Grimshaw, Z. Huang, S. Igl, J. Wang, and W. Dong, *Technical Digest of SSDLTR 2004 (*Direct Energy Professional Society), Diode-3.
3. R. Lammert, M. Osowski, M. Young, S. Oh, and J. Ungar, in *Technical Digest of Solid State and Diode Lasers Technology Review, SSDLTR, 2004* (Direct Energy Professional Society), p. 10.
4. D. Garbuzov, I. Kudryashov, M. Dubinskii, *Appl. Phys. Lett*., **86**, 131115 (2005)
5. L. Shterengas, G.L. Belenky, A. Gourevitch, D. Donetsky, J.G. Kim, R.U. Martinelli, and D. Westerfeld, *IEEE Photon. Tech. Lett.* **16**, 2218, (2004)
6. G. Erbert, A. Barwolff, J. Sebastian, and J. Tomm, Top. Appl. Phys. **78**, 173 (2000).
7. J. G. Endriz *et al.*, *IEEE J. Quantum Electron*. **28**, 952 (1992).
8. S. A. Payne *et al.*, *IEEE J. Sel. Top. Quantum Electron*. **3**, 71 (1997).
9. R. Beach, W. J. Benett, B. L. Freitas, D. Mundinger, B. J. Comaskey, R. W. Solarz, and A. Emanuel, *IEEE J. Quantum Electron*. **28**, 966 (1992).
10. H.Q. Le, G.W. Turner, J.R. Ochoa, *IEEE Photon. Technol. Lett.*, **10**, 663 (1998)
11. J. A. Skidmore, B. L. Freitas, C. E. Reinhardt, E. J. Utterback, R. H. Page, and M. A. Emanuel, *IEEE Photon. Technol. Lett.*, **9**, 1334, (1997)
12. M. Maiorov, R. Menna, V. Khalfin, H. Milgazo, R. Matarese, D. Garbuzov, and J. Connolly, *IEEE Photonics Technol. Lett.* **11**, 961 (1999); M. Maiorov, R. Menna, V. Khalfin, H. Milgazo, A. Triano, D. Garbuzov, and J. Connolly, *Electron. Lett*. **35**, 636 (1999)
13. M. Fukuda, *Reliability and Degradation of Semiconductor Lasers and LEDs* (Boston, MA: Artech House, 1991).
14. B. Laikhtman, A. Gourevitch, D. Westerfeld, D. Donetsky and G. Belenky, submitted in *Semicond. Sc. Technol*. (2005).
15. S.D. Setzler, P.A. Budni, and E.P. Chicklis, OSA Trends in Optics and Photonics, **50**, Advanced Solid-State Lasers, Christopher Marshall, ed. (Optical Society of America, Washington, DC), 309 (2001).
16. S. D. Setzler, K. J. Snell, T. M. Pollak, P. A. Budni, Y. E. Young, E. P. Chicklis, *Opt. Lett*.,**28**, 1787 (2003)
17. D.Z. Garbuzov, R.J. Menna, R.U. Martinelli, J.H. Abeles, J.C. Connolly, *IEE Electron. Lett.* **33**, 1635 (1997).
18. A. Gourevitch, B. Laikhtman, D. Westerfeld, D. Donetsky, G. Belenky, C. W. Trussell, Z. Shellenbarger, H. An, R. U. Martinelli, *J. Appl. Phys*., **97**, 084503, (2005).
19. M. Voss, C. Lier, U. Menzel, A. Barwolff, T. Elsaesser, J. Appl. Phys., **79**, 1170 (1996)